Macromolecules
ARTICLE

Macromolecules **2010**, *43*, 5315–5322 **5315**
DOI: 10.1021/ma100228r

Melting Behavior of Epitaxially Crystallized Polycarprolactone on a Highly Oriented Polyethylene Thin Film Investigated by *in Situ* Synchrotron SAXS and Polarized Infrared Spectroscopy

Yongxin Duan,[†] Jianming Zhang,*[,†] Haibo Chang, Shouke Yan,*[,‡] Chunming Yang,[§] Isao Takahashi,[§] and Yukihiro Ozaki[§]

[†]*Key Laboratory of Rubber-plastics, Ministry of Education, Qingdao University of Science and Technology, Qingdao City 266042, People's Republic of China,* [‡]*State Key Laboratory of Chemical Resource Engineering, Beijing University of Chemistry and Engineer, Beijing 100080, People's Republic of China, and* [§]*School of Science and Technology, and Research Center for Environment Friendly Polymers, Kwansei-Gakuin University, Gakuen, Sanda 669-1337, Japan*

Received January 29, 2010; Revised Manuscript Received May 10, 2010

ABSTRACT: Melting behavior of epitaxially crystallized polycarprolactone (PCL) on a highly oriented polyethylene (PE) substrate was investigated by synchrotron small-angle X-ray scattering (SAXS) and Fourier transform infrared spectroscopy (FTIR). It is found that two dominant crystal thicknesses are clearly identified in the final melting stage around the melting point. In contrast to the normal melting process of polymers, the original PCL crystal and the melt-reorganized one with various lamellar thicknesses are molten and diminished simultaneously. During the melting process, orientations of the residual crystal and ordered all-trans PCL chain are found to be kept. However, the average chain orientation relaxation in the amorphous region is synchronously decreased with the evolution of melting process. A sliding diffusion mechanism was used to explain the melt behavior of PCL on the highly oriented PE substrate.

1. Introduction

The crystallization behavior of polymers has been one of the important topics of polymer science. With the development of modern characterization techniques, such as atomic force microscopy (AFM), X-ray scattering, and neutron scattering, many new observations especially on the microstrucutre/morphology evolution at the early stage of polymer crystallization have recently been disclosed.[1−8] Although these new observations trigger more arguments and discussions on the crystallization mechanism of polymers, no general crystallization mechanism can explain all the experimental observations, and the unification of ideas on polymer crystallization seems to be far from reached. Since it is considered to be a reverse process of polymer crystallization, the melting process has attracted a great deal of attention and a lot of studies have been extensively carried out.[9−16] By investigating the melt process, it certainly enhances our understanding on the polymer crystallization from a different viewpoint.

Crystalline polymers generally exhibit various complex behaviors in melting region, such as intrinsically broad temperature region of 10 °C or more and the parallel occurrence of melting, recrystallization, and reorganization.[9−11] Recently, with an usage of synchrotron radiation, rapid dynamic structure changes during the melting process have been disclosed meticulously by small-angle X-ray scattering (SAXS) and wide-angle X-ray diffraction (WAXD).[12−16] One of the interesting observations is the discontinuous lamellar thickening, in which some of the polymers showed a doubling of lamella thickness[13−16] For explaining the lamellar thickening in the melting process, two major mechanisms have often been adopted: one is the sliding diffusion mechanism that polymer chains in the lamellar crystal slide through the crystal lattice along the chain axis, and the other is the thickening via melt-recrystallization process.[17,18]

By changing the sampling conditions, various polymer and oligomer semi- or single crystals such as polyethylene (PE),[12,13] ultralong alkanes,[14] and poly[(*R*)-3-hydroxybutyrate] and its copolymer[15,16] have been used to study the melting behavior of polymeric substances. However, there have been relatively few reports on the melting behavior of epitaxially crystallized polymers. Recently, we studied the epitaxial crystallization process of polycarprolactone (PCL) and its molecular dynamics on a highly oriented PE substrate by use of time-resolved Fourier transform infrared spectroscopy (FTIR) and wide-angle X-ray diffraction (WAXD).[19] The IR and WAXD results clearly indicated the surface-induced anisotropic chain ordering of PCL in its molten state in the supercooled state on a highly oriented PE substrate, i.e., the occurrence of soft epitaxy. These ordered PCL chain segments then initiate the epitaxial crystallization of PCL on the highly oriented PE substrate under the supercooling conditions. It was indicated that the surface-induced molecular chain ordering reduces the energy barrier for initial stage of crystallization, which in turn largely accelerates the crystallization rate of PCL. These observations strongly suggested the residual chain orientation of PCL still exists on oriented PE even around the melting point where no ordered crystalline PCL lattice is expected. However, no direct evidence of partial ordering in PCL chains has been provided, and the role/mechanism of PE substrate on molecular ordering is still unknown.

So as to answer these questions and accumulate experimental data on molecular ordering, we investigate the melting behavior of epitaxially crystallized PCL, which is sandwiched between two highly oriented PE thin films with time-resolved synchrotron SAXS and polarized FTIR measurements. The use of polarized IR can provide us information about microstructure evolutions

*To whom all correspondence should be addressed: Fax +86-532-84022604, e-mail zjm@qust.edu.cn (J.Z.); e-mail zjm@qust.edu.cn (S.Y.).

Published on Web 05/19/2010

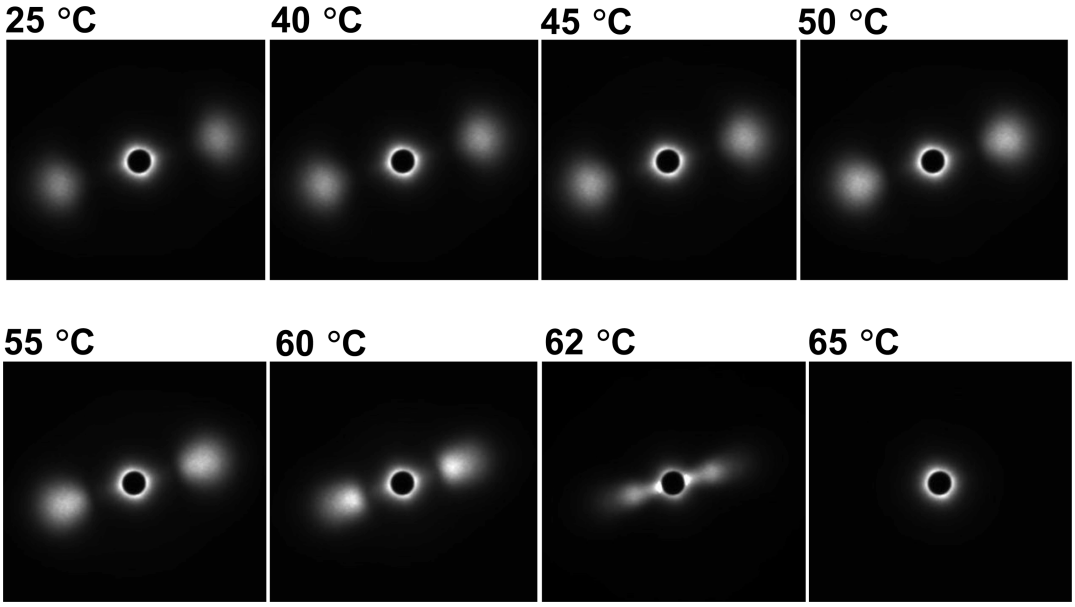

Figure 1. Typical real time 2D-SAXS patterns measured for the PCL epitaxially crystallized on a highly oriented PE thin film in the heating process. The heating rate was 5 °C/min.

of the chain conformation, the intrachain packing, and the chain orientation in both crystalline and amorphous regions, which is an important complement to morphology data of SAXS for figuring out the detailed structure changes in the melting process.[20−24] Our results have shown that a continuous lamellar thickening with unchanged orientation occurs in the whole melting process. Unexpectedly, it is found that the two kinds of dominant crystals with various lamellar thicknesses are molten and diminished simultaneously in the final melting stage. Based on our observations, the unique melting behavior of epitaxially crystallized PCL on a highly oriented PE substrate was explained by the sliding diffusion mechanism.

2. Experimental Section

2.1. Material and Preparation Procedures. Polyethylene (PE) used in the present study was Lupolen 6021 DX (molecular weight $M_w = 6.02 \times 10^5$ and its melting point is 135 °C), produced by BASF AG Ludwigshafen, Germany. Commercial grade PCL, with molecular weight $M_w = 65\,000$, $M_w/M_n = 1.53$, and melting point of 60 °C, was purchased from Sigma-Aldrich Co. The highly oriented PE thin films (30−50 nm) were prepared through a melt-drawing technique introduced by Petermann and Gohil.[25] Detailed orientation information on such thin film is shown in ref 19. To study the melting behavior of PCL crystal on highly oriented PE substrates, a solution-casted PCL thin film with the thickness of about 10 μm was sandwiched between two highly oriented ultrathin PE films with the same chain orientation. Then, the PE/PCL/PE sandwich sample was heated to 85 °C for 15 min and melt-crystallized at 50 °C for 24 h.

2.2. Synchrotron SAXS Measurement. The measurement of 2D-SAXS data was performed at the BL40B2 beam station at SPring-8 (Japan Synchrotron Radiation Research Institute, Hyogo, Japan). The wavelength of the incident X-ray beam was 1.00 Å. A Rigaku R-AXIS IV++ imaging plate system was used as the 2D detector. The sample was packed into an aluminum pan, which was set to a DSC cell (Metlar Toledo FP90). The X-ray exposure time was 10 s for every SAXS measurement and the heating rate of 5 °C/min. In the heating process from 25 to 80 °C, the 2D-SAXS data were collected every 0.8 °C. The SAXS patterns measured were corrected for the background scattering.

2.3. FTIR Spectra. FTIR spectra were measured with a Thermo Nicholet Magna 870 spectrometer equipped with a MCT detector. The normal transmission mode was employed for the IR measurements. For studying the melting behavior of epitaxially crystallized PCL on an oriented PE, the sandwiched sample thus prepared was set on an Instec HCS302 variable temperature cell, which was placed in the sample compartment of the spectrometer. The sample was then heated from 30 to 80 °C with a heating rate of 1 °C/min. During the heating process, polarized FTIR spectra of the specimens were recorded at a 1 °C interval with a 1 min interval with the polarized beam parallel and perpendicular to the PE chain direction, respectively. The spectra were obtained by coadding 16 scans at a 2 cm^{-1} resolution.

2.4. Data Analysis of SAXS and FTIR. The two-dimensional (2D) SAXS patterns seen during this experiment consist of only one main feature, which is the two-point pattern as shown in Figure 1. The two points move inward toward the beam stop with increasing temperature. This broad reflection indicates the existence of a partially oriented stacked lamellar structure in our sample.

In order to increase the signal-to-noise ratio in the resulting scattering curves, the 2D SAXS images were converted to one-dimensional (1D) profiles by circularly averaging with a Fit2d software package. Then, the Lorentz correction was applied to the integrated 1D profile after subtraction of background for getting the accurate values of long periods as described in references for anisotropic system.[15,16,26,27]

For isotropic system with periodic structure, the Lorentz correction is often used to correct the intensities of X-ray scattering in order to obtain structure factors. Meanwhile, this correction reduces the intensities to zero at zero diffraction angle so that the accurate values of long periods can be read.

However, for partially oriented system, it should be mentioned that the Lorentz correction was thought to be suitable for 1D meridional intensity distribution rather than the total integrated intensity of the 2D SAXS pattern by some other researchers.[28−30] In this work, we think that our qualitative conclusion on the change of long periods will be not much affected by the Lorentz correction on the circularly integrated curve. Meanwhile, for comparing with the SAXS study of melting behavior of polymer by Iwata et al.,[15,16] we therefore take the same procedure of the Lorentz correction as described by them.

The intensities of IR bands were automatic calculated by a numerical data processor program for vibrational spectroscopy,

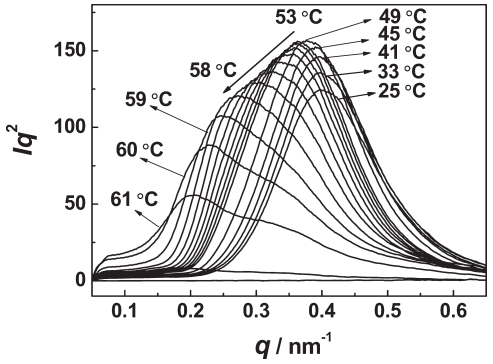

Figure 2. Lorentz-corrected SAXS profiles evaluated from Figure 1.

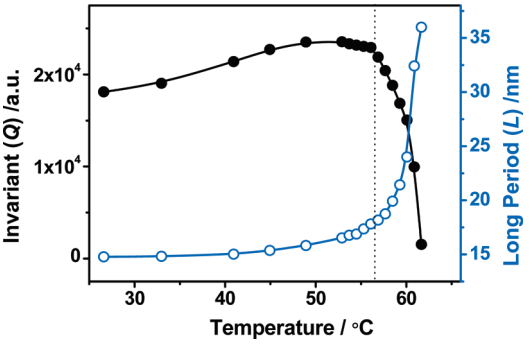

Figure 3. Temperature dependence of the invariant Q and long period L calculated from Figure 2.

Spina Version 3, which was developed by Yukiteru Katsumoto in the Ozaki Group of Kwansei Gakuin University.

3. Results and Discussion

3.1. Morphology Evolution during Heating Monitored by Time-Resolved SAXS Measurement. Figure 1 shows some of the typical real time 2D-SAXS patterns for sandwiched PCL between highly oriented PE thin films. The SAXS signals should be mainly come from PCL rather than PE thin films because the thickness of PE film (30−50 nm) used here are far smaller than that of PCL film (≈10 μm). Meanwhile, the SAXS pattern taken at 65 °C as shown in Figure 1, in which the PCL is molten and PE is still in the crystalline state, also suggests that no obvious signal can be observed from such PE thin film. At room temperature, two point patterns across the direct beam position indicate that the lamellar stacking of PCL is highly oriented. The tilting of the line along the two scattering points with the meridian direction is presumably due to the tilting of the sample in the heater. The corresponding Lorentz-corrected one-dimensional profiles are shown in Figure 2, in which $q = (4\pi/\lambda) \sin \theta$, where 2θ is the scattering angle and λ is the wavelength of the X-rays.

As shown in Figure 2, the original scattering peak gradually shifted to a lower scattering angle during heating from 25 to 57 °C. Interestingly enough, two overlapped scattering peaks were observed at temperatures close to the melting point (ca. 60 °C). We will discuss this pointer later.

From the one-dimensional profile, the most probable long period (L) was estimated using Bragg's law to analyze the position of scattering maximum in the Lorentz-corrected intensity profile, and the scattering invariant (Q) was calculated using eq 1.[27]

$$Q = \int_{q1}^{q2} I(q) q^2 \, dq \qquad (1)$$

In eq 1, the values of $q1$ and $q2$ represent the limitations of the experimental setup.

The invariant Q and the apparent long period L were plotted against temperature as displayed in Figure 3. On heating, the invariant Q increases first and goes through a maximum around 50 °C. With temperature close to the melting point of PCL (60 °C), a rapid decreasing of the invariant Q is observed.

For the two-phase crystalline−amorphous model with volume fraction of crystals φ_c and electron density difference $\Delta\rho$ between crystalline phase and amorphous phase (electron/m^3), the invariant Q is presented as[9]

$$Q = \varphi_c(1 - \varphi_c)\Delta\rho^2 \qquad (2)$$

As indicated by eq 2, the invariant Q is not only related to the volume fraction of φ_c but also related to $\Delta\rho$. Before the main melting process, the change in crystallinity is relatively minor and its effect on $\varphi_c(1 - \varphi_c)$ is thus negligible. Therefore, the initial increasing of invariant Q should mainly be caused by the change in $\Delta\rho$. As discussed in ref 9, increased temperature usually enhances the electron density difference $\Delta\rho$. The invariant Q is also directly proportional to the integrated intensity of the scattering peak in the one-dimensional Iq^2-q curve. Therefore, the initial increasing of invariant Q in Figure 3 or the intensity increasing in Figure 3 is likely to be caused by the temperature effect and is not related to the structural change.

However, in the heating process from 50 to 57 °C, the subtle decrease of the invariant Q together with the obvious increasing in long period L (from 15.9 to 18.7 nm) suggests that some structure changes take place. We have noticed that 50 °C is the crystallization temperature of our PCL sample for heating, above which structural relaxation or recrystallization is usually expected. We will return to this point again combined with the IR data later.

Most interestingly, in the final melting process from 57 to 62 °C, the long period L increases largely (from 18.7 to 36.5 nm, corresponding to ca. 100% increase). During the melting process of semicrystalline polymer, the increase of long period is usually caused by two possibilities. One is the lamellar thickening, and the other is the increase of amorphous region in between the lamellae due to melting. Of note, the neat PCL will be totally molten at temperature before 60 °C. However, as shown in Figure 2, two points SAXS pattern of PCL epitaxial crystallized on PE thin film can still be clearly observed at 62 °C, which suggests that ordered crystalline structure with larger lamellar thickness exists at temperature above the normal melting point of PCL. Recently, by the measurement of AFM, it is found that the lamellar thickness of PCL can reach ca. 55 nm after annealing the epitaxial crystallized PCL on highly oriented PE substrate for 6 days at 60 °C.[31] Therefore, we consider that the increase of long period observed by SAXS data here corresponds to the lamellar thickening. Actually, the lamellar thickening during the melting process have been observed by many researchers.[13−18]

3.2. Time-Resolved Polarized FTIR Measurement. Figure 4 shows the polarized IR spectra of the epitaxially crystallized PCL on a highly oriented PE substrate in the region of 3050−700 cm^{-1}. Because of the saturation of C=O stretching bands, the 1800−1600 cm^{-1} region is omitted in Figure 4. Since the thickness of the PE substrate is very thin, ca. 30−50 nm, no signal from PE is visible. The obvious intensity differences between the perpendicular and parallel bands suggest that the PCL chains are highly oriented, which is fully consistent

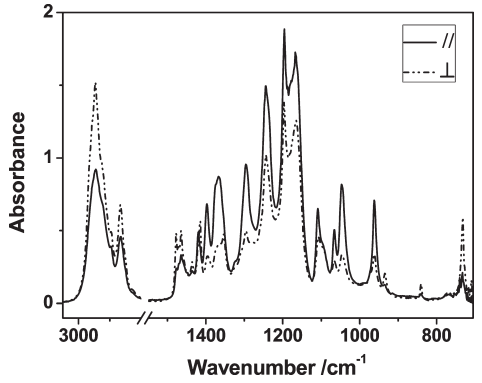

Figure 4. Polarized transimission IR spectra of PCL epitaxially crystallized on a highly oriented PE thin film in the region of 3050−700 cm^{-1}. The spectra were measured at room temperature.

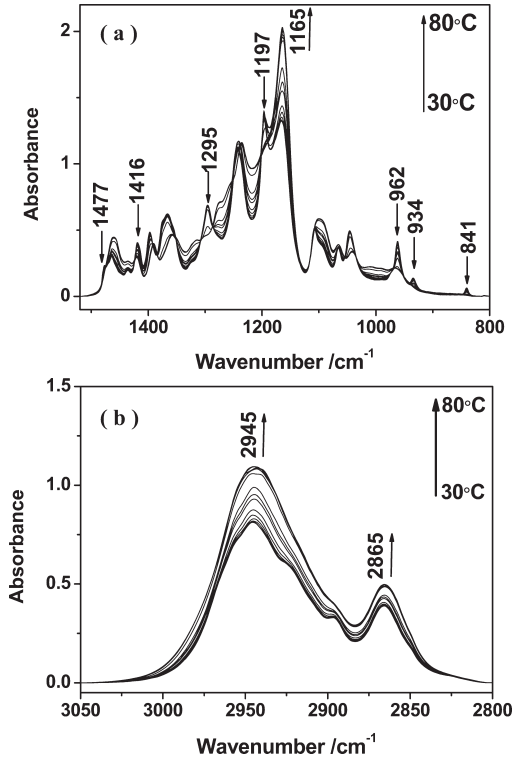

Figure 5. IR spectral evolution of PCL epitaxially crystallized on a highly oriented PE thin film during the heating process from 30 to 80 °C in the region of 1500−800 cm^{-1} (a) and 3050−2800 cm^{-1} (b). The heating rate was 1 °C/min, and the spectra are arranged with a 1 °C interval. IR transmission mode was performed for the sandwiched sample.

with our SAXS data. By examining the intensity differences in Figure 4, it is easy to identify the perpendicular and parallel bands. Figure 5 shows the temperature-dependent IR spectra of our sample from 30 to 80 °C. By this set of spectra, we can distinguish crystalline bands and amorphous bands because the semicrystalline sample will totally turn to an amorphous state at the temperature above the melting point of PCL (ca. 60 °C), where only amorphous bands appear and the crystalline bands disappear.

It is found that the complete band assignments of PCL have not been available yet.[32−35] However, considering the simple molecular structure of PCL as depicted in Scheme 1, which comprises the short alkyl chain and the ester bond, a tentative assignment may be given by referring the assignments

Scheme 1. Chemical Structure of PCL

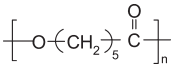

Table 1. Band Assignments of PCL

wavenumber/cm^{-1}	assignment		polarization[a]
2945	$\nu_{as}(CH_2)$	amorphous	⊥
2865	$\nu_s(CH_2)$	crystalline	⊥
1477	$\delta(CH_2)$[b]	crystalline	⊥
1295	$\nu(CO) + \nu(CC)$	crystalline	∥
1245	$\nu_{as}(COC)$	crystalline	∥
1165	$\nu_s(COC)$	amorphous	∥
962	$(C-C) + r(CH_2)$[b]	crystalline	∥
934		crystalline	⊥
841		crystalline	⊥
731	$\gamma(CH_2)$	crystalline	⊥

[a] ∥ and ⊥ indicate that the electric vector of incident infrared beam is parallel and perpendicular to the chain direction, respectively. [b] Tentative band assignment by us.

for the IR spectra of PE, nylon, etc.[36,37] The band assignments given in the literature[34−36] together with our tentative assignments are summarized in Table 1. Among them, bands at 2945, 2865, 1477, and 731 cm^{-1} are related to the localized vibrations of CH_2 groups, whereas the bands at 1295, 1245, and 1165 cm^{-1} are associated with the localized vibrations of C−O−C bond.

In our previous paper, on the basis of the band assignment of similar orthorhombic PCL crystal with cell parameters $a = 0.747$, $b = 0.498$, and $c = 1.705$ nm and that of PE crystal with $a = 0.74$, $b = 0.494$, and $c = 0.253$ nm, especially for the a and b unit cell dimensions,[38,39] we have discussed that the band at 731 cm^{-1} and another weak band around 710 cm^{-1} originate from factor group splitting due to the intermolecular interaction of the CH_2 sequences packed in an orthorhombic unit cell just as in the case of PE crystals. In fact, it is also rational to speculate that the $\delta(CH_2)$ band at 1477 cm^{-1} has the same origin as that of the $\gamma(CH_2)$ band at 731 cm^{-1} because the band splitting is observed not only for $\delta(CH_2)$ and but also for $\gamma(CH_2)$ vibration mode in the orthorhombic unit cell of PE. That is, both the bands at 731 and 1477 cm^{-1} are associated with the dense chain packing in the PCL crystal. In other words, they are the true crystalline sensitive bands. In this paper, in order to perform the real-time FTIR measurement for the fast melting process, the liquid nitrogen cooled MCT detector was used so that the limited lowest frequency is a little overlapped with the 731 cm^{-1}. Therefore, we will use the band at 1477 cm^{-1} as a marker band to follow the change in crystalline structure, especially the changes in chain packing during the melt process.

In the spectral region of 1000−800 cm^{-1} (Figure 5), there are several crystalline bands with sharp peak profiles located at 962, 934, and 841 cm^{-1}, which decrease in intensities upon heating and disappear totally in the molten state of PCL. Usually, the vibration modes in the lower frequency region of polymers are assigned to the chain backbone vibration. Meanwhile, we noticed that the bands observed in this spectra region for nylons and *n*-alkane molecules are named as the so-called progression bands, which are assignable to the CH_2 rocking and C−C stretching modes of methylene sequence of finite chain length. Therefore, we tentatively propose that the three bands at 962, 934, and 841 cm^{-1} are sensitive to the all-trans TTTT conformation ordering of the $-CH_2-CH_2-CH_2-CH_2-CH_2-$ methylene sequence in the crystal structure of PCL.

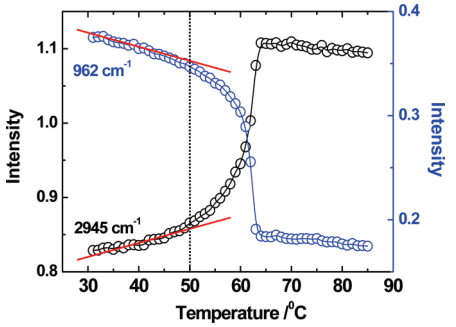

Figure 6. Intensity changes of PCL amorphous (2945 cm^{-1}) and crystalline (962 cm^{-1}) bands during the heating process of PCL epitaxial crystallized on highly oriented PE thin film from 30 to 80 °C.

As shown in Figure 5, the bands at 2945 and 1165 cm^{-1} increase in intensities obviously during the melting process. Thus, it is rational to assign them as the amorphous bands. However, the large absorption coefficient of the ν_s(COC) vibration leads to strong absorption intensity (~2) for our sample, which could not obey the Beer−Lambert law well. Therefore, we only use the $\nu_{ss}(CH_2)$ band at 2945 cm^{-1} to perform the quantitative analysis for the amorphous region.

Intensity changes of PCL amorphous (2945 cm^{-1}) and crystalline (962 cm^{-1}) bands during the heating process from 30 to 80 °C for epitaxially crystallized PCL on the highly oriented PE substrate are depicted in Figure 6. Upon heating, especially in the melting temperature region (around 60 °C), the synchronous changes of the two bands illustrate the crystal-to-amorphous phase transition very well. However, it should be mentioned that the absorption coefficient of IR band is a function of temperature. Usually, it will decrease with increasing temperature. Thus, the gradual linear increasing of the amorphous band or the decreasing in the crystalline band at the initial heating process (< 50 °C) as shown in Figure 6 should not be considered as the structure changes but caused mainly by the decreasing of the IR absorption coefficient with increasing temperature. Above 50 °C, the rate of changes in intensity of the two bands rapidly varies with temperature. It indicates that some structural changes take place. The drastic decreasing of the crystalline band at 962 cm^{-1} is observed above 50 °C. Meanwhile, in the SAXS data (Figure 3), invariant Q also starts to decrease with heating temperature above this temperature. Therefore, these data clearly show that the melting process of the sample starts from 50 °C. Figure 6 also shows that the sample is finally molten at ca. 63 °C, which is totally consistent with the SAXS data.

The temperature-dependent polarized IR spectra for the sample in various spectral regions are shown in Figures 7−9. For comparison, the temperature-dependent IR spectra obtained without the polarizer are also provided. In the spectral region of 1500−1400 cm^{-1} (Figure 7), the change of the crystalline sensitive band at 1477 cm^{-1} clearly forms a sharp shoulder peak in the perpendicular spectra.

In the spectral region of 1350−1110 cm^{-1} (Figure 8), the changes of three broad peaks (1295, 1245, and 1197 cm^{-1}) associated with the C−O−C stretching vibration are identified especially in the parallel spectra. Obviously, the bands in this spectral region are heavily overlapped, and there is some peak shifting in the melting process. In contrast, in the spectral region of 980−800 cm^{-1} (Figure 9), the progressive bands (962, 934, and 841 cm^{-1}) associated with the all-trans TTTT conformation of the $-CH_2-CH_2-CH_2-CH_2-CH_2-$ methylene sequence are well resolved in both parallel and perpendicular bands, and their peak positions are unchanged

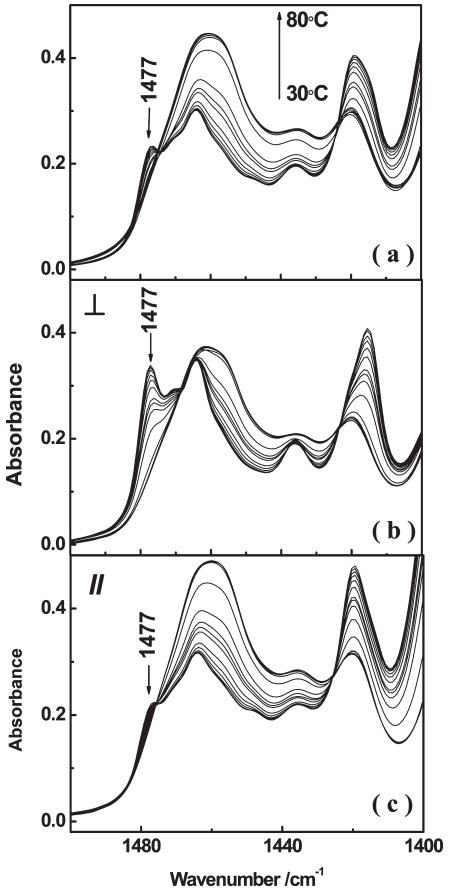

Figure 7. No polarized (a), perpendicular (b), and (c) parallel polarzied IR spectral evolution of epitaxially crystallized PCL on oriented PE thin film during the heating process from 30 to 80 °C in the region of 1500−1400 cm^{-1}.

throughout the temperature range investigated. Therefore, the bands at 1477 cm^{-1} and 962, 934, and 841 cm^{-1} are suitable for quantitative analysis.

Their intensity changes of these bands as a function of temperature derived from the perpendicular spectra of Figure 7−9 are shown in Figure 10. With increasing the temperature, the monotonic decrease of these crystalline bands is observed. It should be noted that not only the melting of PCL crystal but also the orientation change can induce the intensity changes in these temperature-dependent polarized IR spectra.

The extent of chain orientation is usually described by an orientation function f defined as[20]

$$f = \frac{R-1}{R+2}\frac{2}{3\cos^2\alpha - 1}$$

where α is the angle between the chain axis and the transition moment associated with the infrared band used for the measurement. For simplify, α is taken as 0°or 90° for the parallel or perpendicular bands, respectively. R is the measurable infrared dichroic ratio defined as $R = A_{\parallel}/A_{\perp}$, with $A_{\parallel}$ and $A_{\perp}$ reflecting the absorbance when the infrared beam was polarized parallel and perpendicular to the chain direction, respectively.

The variation of orientation function for crystalline sensitive band at 1477 cm^{-1}, the conformation sensitive bands at 962, 934, and 840 cm^{-1}, and the amorphous band at 2945 cm^{-1} as a function of temperature are summarized in Figure 11. It is quite obvious that the orientations of the

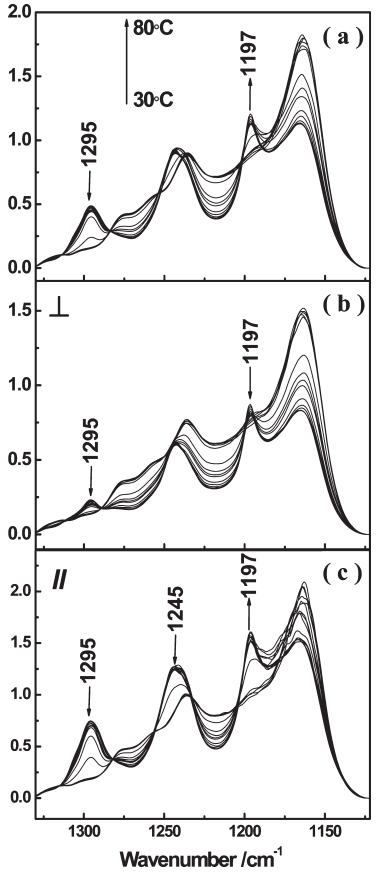

Figure 8. No polarized (a), perpendicular (b), and (c) parallel polarzied IR spectral evolution of epitaxially crystallized PCL on oriented PE thin film during the heating process from 30 to 80 °C in the region of 1330−1120 cm^{-1}.

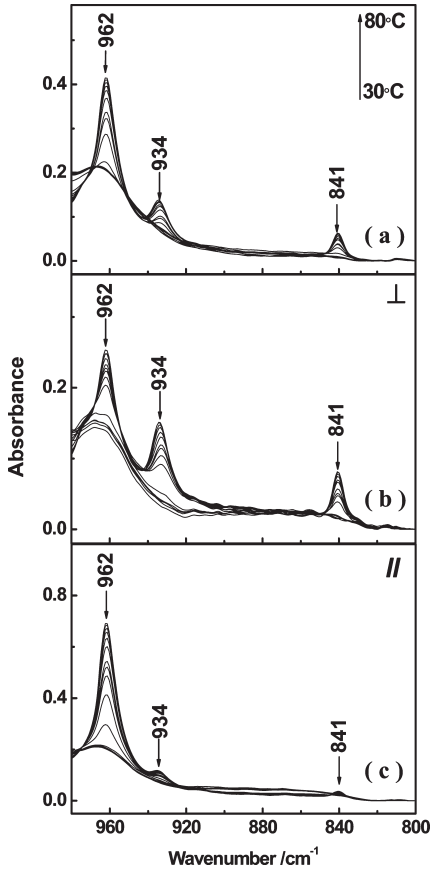

Figure 9. No polarized (a), perpendicular (b), and (c) parallel polarzied IR spectral evolution of epitaxially crystallized PCL on oriented PE thin film during the heating process from 30 to 80 °C in the region of 980−800 cm^{-1}.

remaining crystal and ordered all-trans chain conformation of PCL show almost no change below 62 °C, whereas the chain orientation in the amorphous region is continuously relaxed with increasing the temperature in the melting process.

4. Discussion

By combining the temperature-dependent changes of invariant Q (Figure 3) and that of the crystalline IR band (Figure 6), it can be concluded that two melting stages can be identified for the broad temperature region (50−63 °C) of epitaxial crystallized PCL on the highly oriented PE. One is the premelting process between 50 and 57 °C, and the other is the main melting process above 58−63 °C. In the final melting stage around the melting point, two dominant crystal thicknesses are clearly identified. As an example, the curve fitting was performed on the SAXS profile measured at 60 °C. As depicted in Figure 12, two scattering peaks were resolved at $q = 0.22\ nm^{-1}$ ($L = 28.5$ nm) and $q = 0.32\ nm^{-1}$ ($L = 19.6$ nm).

All the SAXS profiles measured in the final melting stage were analyzed by the same curve fitting procedure. As shown in Figure 13, the original long period (L_0) is split into two in the final melting stage. The long periods with smaller values (L_1) are comparable with those of the original long period. Therefore, it is rational to assign the crystal lamella with smaller L_1 is the remaining crystal of the original lamella and the crystalline lamella with larger long period (L_2) is the newly developed, melt-reorganized ones.

Usually, the half-width ($\Delta\omega$) of the scattering peak is inversely proportional to the ordering extent of period structure. On the

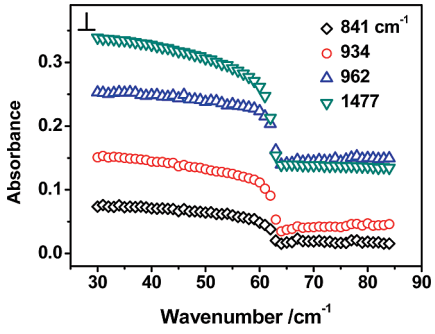

Figure 10. Intensity changes of various bands calculated from Figures 7−9 as a function of temperature from 30 to 80 °C.

basis of the change of the half-width of the curve fitted scattering peaks, it is found that the original one ($\Delta\omega_1$) becomes less ordering, whereas the ordering of the melt-reorganized one ($\Delta\omega_2$) increase gradually with increasing temperature. The subtle increasing in long period and decreasing in crystalline ordering for the original crystal suggest that the lateral melting may be dominated in the final melting stage. Unexpectedly, it is found that the original and the melt-reorganized crystal are molten and diminished simultaneously as evidenced by their synchronized intensity decreasing with heating.

At the end of the melting process, the conversion from a peaked to a monotonic SAXS pattern is often observed for polyethylene,[40] sydiotactic polypropylene,[41] and poly(3-hydroxybutyrate).[15,16,42] It suggests that the lamellar with smaller lamellar thicknesses are molten first, and the isolated lamellae with

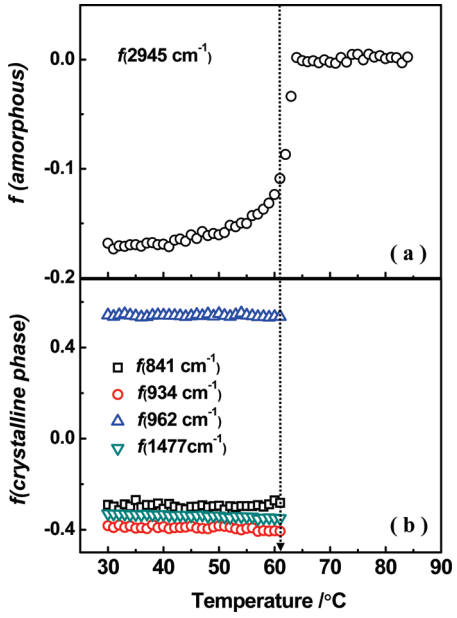

Figure 11. Temperature dependence of the orientation function calculated by the amorphous band at 2945 cm^{-1} (a) and crystalline sensitive bands at 841, 934, 962, and 1344 cm^{-1} (b) of epitaxially crystallized PCL on a highly oriented PE thin film during the heating process from 30 to 80 °C.

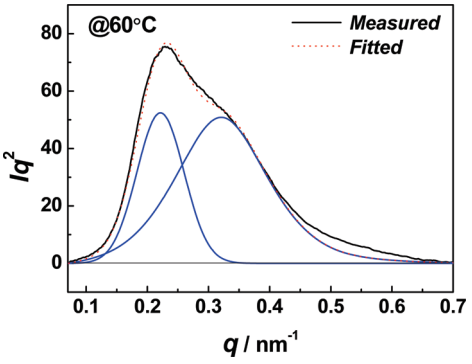

Figure 12. An example of the curve fitting for the SAXS profiles measured at 60 °C.

larger lamellar thicknesses are present even at the end of the melting stage. Such an explanation seems to be quite reasonable because the melting point of the lamellae crystal is proportional to the lamellar thickness. However, how to explain our above observation for epitaxial crystallized PCL on highly oriented PE substrate?

As mentioned in the Introduction, two major mechanisms have often been adopted to explain the lamellar thickening phenomenon in the melting process. One is the sliding diffusion mechanism that polymer chains in the lamellar crystal slide through the crystal lattice along the chain axis, and the other is the thickening by the melt-recrystallization process.[15−18] Usually, the melt-crystallized crystal is more stable than the original one. However, in our case, the original crystal and the melt-reorganized one are molten simultaneously. Therefore, the conventional melt-crystallization mechanism may not describe our observation well. Because of the soft epitaxy effect by the highly oriented PE substrate and the enhanced chain mobility, it can be considered that melt-reorganized stacked structure is formed by the sliding diffusion mechanism. That is, in the final melt stage, lateral melting and sliding diffusion induce the structure reorganization. Under such circumstances, the lateral interchain

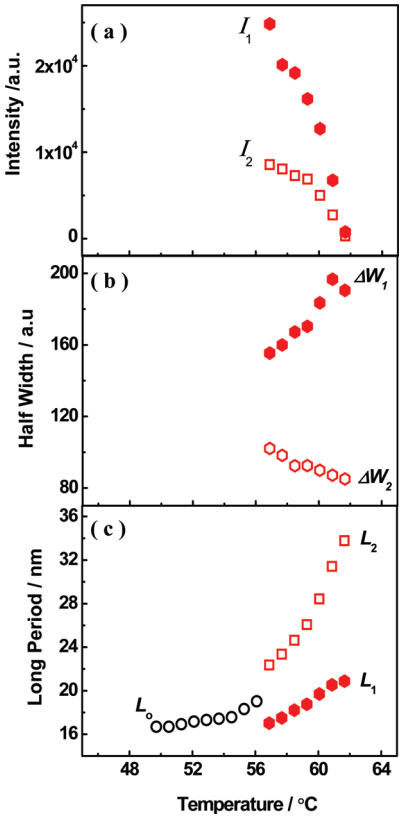

Figure 13. Intensities (a), half-widths (b), and long periods (c) as a function of temperature calculated by curve fitting methods for the SAXS profiles depicted in Figure 2.

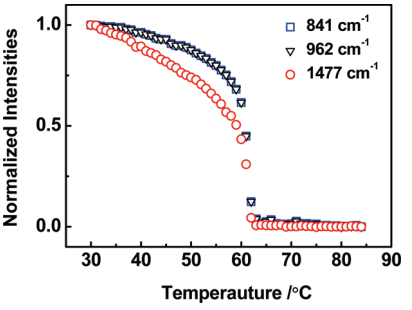

Figure 14. Intensity changes of crystalline sensitive band (1477 cm^{-1}) and conformation sensitive bands (962 and 840 cm^{-1}) during the heating process of PCL epitaxially crystallized on an oriented PE thin film from 30 to 80 °C without polarizer.

interactions between the original crystal and the newly formed one are the similar. Therefore, both crystals collapse at the same time with increasing the temperature.

Figure 14 shows the intensity changes of the crystal sensitive band at 1477 cm^{-1} and conformation-sensitive bands at 840 and 962 cm^{-1} derived from the temperature-dependent IR spectra without polarizer. It is found that the decreasing rate of the crystalline sensitive band is much larger than those of the conformation-sensitive bands. As mentioned previously, the band at 1477 cm^{-1} is caused by the interchain packing of the ordered CH_2 sequences. Usually, thermal expansion of the lattice along *a* or *b* axis in the crystal will occur in the heating process. Therefore, the drastic decrease in intensity of this band indicates that the interchain interaction becomes weak and the ordered chain conformation is stable before the final collapse of the crystal. With the decreasing in the interchain interaction and the increasing in the chain mobility, chain sliding will take place with

increasing temperature. Moreover, sliding diffusion along the *c* axis is facilitated by the directional effect of the highly oriented PE substrate.

5. Conclusion

The melting behavior of epitaxially crystallized polycarprolactone (PCL) on a highly oriented PE substrate was investigated by synchrotron small-angle X-ray scattering (SAXS) and Fourier transform infrared spectroscopy (FTIR). A continuous lamellar thickening behavior upon heating to the melting temperature region of PCL was observed. In the final melting stage around the melting point of PCL, two dominant crystal thicknesses are identified by the curve fitting on SAXS profiles. In contrast to the normal melting process of polymers, it is found that the original crystal and the melt-reorganized one with various lamellar thicknesses are molten and diminished simultaneously. During the melting process, the orientation of the remained crystal and the ordered all-trans PCL chain are kept. However, the average chain orientation relaxation in the amorphous region is synchronized with the evolution of melting process. These observations suggest that there is an interface interaction between the PCL crystal and the highly oriented PE substrate. However, the ordered chain and the chain orientation in the amorphous region cannot be stabilized at the temperatures close to the melting point where the entropic effect is more dominant than the soft epitaxy effect from the substrate.

Acknowledgment. Jianming Zhang thanks the helpful discussion with Prof. Liangbin Li and Prof. Zhigang Wang on the SAXS data. The financial support from Shangdong Province Science Fund for Distinguished Young Scholars (JQ200905), Taishan Mountain Scholar Constructive Engineering Foundation (TS20081120), Doctoral Fund of Qingdao University of Science and Technology, and Open Project of Key Laboratory of Rubber-Plastics, Ministry of Education, is greatly appreciated. The synchrotron radiation experiments were performed at the BL40B2 in SPring-8 with the approval of the Japan Synchrotron Radiation Research Institute (JASRI) (Proposal No. 2008A1649).

References and Notes

(1) Imai, M.; Kaji, K.; Kanaya, T.; Sakai, Y. *Phys. Rev. B* **1995**, *52*, 12696–12704.
(2) Lei, Y.; Chan, C.; Li, J.; Ng, K.; Wang, Y.; Jiang, Y.; Li, L. *Macromolecules* **2002**, *35*, 6751–6753.
(3) Strobl, G. *Prog. Polym. Sci.* **2006**, *31*, 398–442.
(4) Kimata, S.; Sakurai, T.; Nozue, Y.; Kasahara, T.; Yamaguchi, N.; Karino, T.; Shibayama, M.; Kornfield, J. A. *Science* **2007**, *316*, 1014–1017.
(5) Li, L. B.; De Jeu, W. H. *Adv. Polym. Sci.* **2005**, *181*, 75–120.
(6) Muthukumar, M. *Adv. Polym. Sci.* **2005**, *191*, 241–274.
(7) Reiter, G.; Strobl, G. *Progress in Understanding of Polymer Crystallization*; Springer: Berlin, Germany, 2007.
(8) Strobl, G. *Eur. Phys. J. E* **2000**, *3*, 165–183.
(9) Crist, B. *Macromolecules* **2003**, *36*, 4880–4890.
(10) Wunderlich, B. *Macromolecular Physics*; Academic Press: New York, 1976; Vol. *3*.
(11) Toda, A.; Kojima, I.; Hikosaka, M. *Macromolecules* **2008**, *41*, 120–127.
(12) Rastogi, S.; Lippits, D. R.; Peters, G. M.; Graf, R.; Yao, Y.; Spiess, H. *Nature Mater.* **2005**, *4*, 635–641.
(13) Rastogi, S.; Spoelstra, A. B.; Goossens, J. G. P.; Lemstra, P. J. *Macromolecules* **1997**, *30*, 7880–7889.
(14) Ungar, G.; Zeng, X. *Chem. Rev.* **2001**, *101*, 4157–4188.
(15) Sawayanagi, T.; Tanaka, T.; Iwata, T.; Abe, H.; Doi, Y.; Ito, K.; Fujisawa, T.; Fujita, M. *Macromolecules* **2006**, *39*, 2201–2208.
(16) Sawayanagi, T.; Tanaka, T.; Iwata, T.; Abe, H.; Doi, Y.; Ito, K.; Fujisawa, T.; Fujita, M. *Macromolecules* **2007**, *40*, 2392–2399.
(17) Dreyfuss, P.; Keller, A. *J. Macromol. Sci., Phys.* **1970**, *B4*, 811–836.
(18) Mandelkern, L.; Sharma, R. K.; Jackson, J. F. *Macromolecules* **1969**, *2*, 644–647.
(19) Yan, C.; Li, H. H.; Zhang, J. M.; Ozaki, Y.; Shen, D. Y.; Yan, D. D.; Shi, A. C.; Yan, S. K. *Macromolecules* **2006**, *39*, 8041–8048.
(20) Chalmers, J. M.; Hannah, R. W.; Mayo, D. W. Spectra-structure correlations: Polymer spectra. In *Handbook of Vibrational Spectroscopy*; Chalmers, J. M., Griffiths, P. R., Eds.; John Wiley & Sons: Chichester, UK, 2002; Vol. *4*, pp 2441−2443.
(21) Koenig, J. L. *Spectroscopy of Polymer*, 2nd ed.; Elsevier Science Inc.: New York, 1999.
(22) Zhang, J. M.; Duan, Y. X.; Sato, H.; Tsuji, H.; Noda, I.; Yan, S. K.; Ozaki, Y. *Macromolecules* **2005**, *38*, 8012–8021.
(23) Kobayashi, M.; Sakashita, M. *J. Chem. Phys.* **1992**, *96*, 748–760.
(24) Cao, W. Y.; Tashiro, K.; Hanesaka, M.; Takeda, S.; Masunaga, H.; Sasaki, S.; Takata, M. *J. Phys. Chem. B* **2009**, *113*, 2338–2346.
(25) Petermann, J.; Gohil, R. M. *J. Mater. Sci.* **1979**, *14*, 2260–2264.
(26) Kumaraswamy, G.; Verma, R. K.; Kornfield, J. A.; Yeh, F. J.; Hsiao, B. S. *Macromolecules* **2004**, *37*, 9005–9017.
(27) Wang, Z. G.; Xia, Z. Y.; Yu, Z. Q.; Chen, E. Q.; Sue, H. J.; Han, C. C.; Hsiao, B. S. *Macromolecules* **2006**, *39*, 2930–2939.
(28) Samon, J. M.; Schultz, J. M.; Hsiao, B. S. *Polymer* **2000**, *41*, 2169–2182.
(29) Wu, J.; Schultz, J. M. *Macromolecules* **2000**, *33*, 1765–1777.
(30) Ruland, W. *Colloid Polym. Sci.* **1978**, *256*, 932–936.
(31) Chang, H. B.; Zhang, J. M.; Li, L.; Wang, Z. H.; Yang, C. M.; Takahashi, I.; Ozaki, Y.; Yan, S. K. *Macromolecules* **2010**, *43*, 362–366.
(32) Takahashi, T.; Teraoka, F.; Tsujimoto, I. J. *Macromol. Sci., Phys.* **1976**, *B12*, 303.
(33) Coleman, M. M.; Zarian, J. *J. Polym. Sci., Polym. Phys.* **1979**, *17*, 837–850.
(34) Hubble, D.; Cooper, S. *J. Polym. Sci., Polym. Phys. Ed.* **1977**, *15*, 1143–1161.
(35) Elzein, T.; Nasser-Eddine, M.; Delaite, C.; Bistac, S.; Dumas, P. *J. Colloid Interface Sci.* **2004**, *273*, 381–387.
(36) Krimm, S.; Liang, C. Y.; Sutherland, G. B. B. M. *J. Chem. Phys.* **1956**, *25*, 549–562.
(37) Yoshioka, Y.; Tashiro, K. *J. Phys. Chem. B* **2003**, *107*, 11835–11842.
(38) Chatani, Y.; Tadokoro, H.; Yamashita, Y. *Polym. J.* **1970**, *1*, 555–562.
(39) Bittiger, H.; Marchessault, R. H.; Niegisch, W. D. *Acta Crystallogr.* **1970**, *B23*, 1923.
(40) Vonk, C. G.; Koga, Y. *J. Polym. Sci., Polym. Phys. Ed.* **1985**, *23*, 2539–2551.
(41) Schmidtke, J.; Strobl, G.; Thurn-Albrecht, T. *Macromolecules* **1997**, *30*, 5804–5821.
(42) Rule, R. J.; Liggat, J. J. *Polymer* **1995**, *36*, 3831–3840.